



RESEARCH ARTICLE

10.1002/2015RS005785

Special Section:

URSI AT-RASC (Atlantic Radio Science Conference)

Key Points:

- The ionospheric dynamics is highly variable at the low latitudes
- Variations in EEJ control the ionization levels at low latitudes
- Localized effects contribute to ionospheric dynamics during storms

Correspondence to:

O. J. Olwendo,
castrajoseph@yahoo.com

Citation:

Olwendo, O. J., Y. Yamazaki, P. J. Cilliers, P. Baki, and P. Doherty (2016), A study on the variability of ionospheric total electron content over the East African low-latitude region and storm time ionospheric variations, *Radio Sci.*, 51, doi:10.1002/2015RS005785.

Received 3 AUG 2015

Accepted 15 AUG 2016

Accepted article online 16 AUG 2016

A study on the variability of ionospheric total electron content over the East African low-latitude region and storm time ionospheric variations

O. J. Olwendo¹, Yosuke Yamazaki², P. J. Cilliers^{3,4}, P. Baki⁵, and P. Doherty⁶

¹School of Pure and Applied Sciences, Department of Mathematics and Physics, Pwani University, Kilifi, Kenya, ²Department of Physics, Lancaster University, Lancaster, UK, ³Space Science Directorate, South African National Space Agency, Hermanus, South Africa, ⁴Department of Electrical Engineering, University of Cape Town, Cape Town, South Africa, ⁵School of Pure and Applied Sciences, Department of Physics, Kenya Technical University, Nairobi, Kenya, ⁶Institute for Scientific Research, Boston College, Newton, Massachusetts, USA

Abstract The variation of total electron content (TEC) derived from the International Global Navigation Satellite Systems Service receiver (formerly IGS) over the East African low-latitude region from up to 12 observation stations for the period 2012 was analyzed. The diurnal and annual TEC contour plots generated from data over the region show that the equatorial anomaly crests manifest remarkable seasonal variations. The crest of the equatorial ionization anomaly is fully formed and yields the maximum values of TEC during the equinoxes (March/April and September/October) and minimum in the solstice (June/July and November/December). The results of this observation show that the crest develops between 12:00 and 16:00 LT and is greatly dependent on the time when the ionosphere is uplifted at the dip equator via the $E \times B$ drift force. The postsunset TEC enhancements at stations away from dip equator depict the ionospheric plasma density diffusion (flow) from the dip equator leading to the formation of ionization anomaly crests that lasts for few hours after the sunset local time. The ionospheric response to the strong geomagnetic storm of the March 2015 has also been examined. The ionospheric response to the geomagnetic storms has shown a strong thermosphere-ionosphere coupling. The negative storm effect that occurred over the anomaly crest region is more likely due to the composition disturbances associated with high energy deposits.

1. Introduction

The ionosphere is defined as the region of Earth's atmosphere which ranges in height above the surface of the Earth from approximately 60 to 1000 km [Xu *et al.*, 2012] and has sufficient electron density to influence the propagation of electromagnetic radio frequency waves. The ionosphere is thus a dispersive medium for electromagnetic waves and therefore induces a time delay in transionospheric radio signals such as those of the GPS satellite signals [Davies, 1990; Garner *et al.*, 2008]. Because this time delay is dispersive, it can be estimated by differencing the the delay and phase at the two different frequencies. At present, measurement of total electron content (TEC) values using dual-frequency GPS receivers has become a reliable and cost-effective method of probing the thermosphere-ionosphere system. TEC is an important ionospheric characteristic for planning and operation of satellite navigation and communication system since it is directly related to ionospheric electron density, which is the major source of signal degradation. At the low latitudes the largest electron densities are found to peak on either side of the geomagnetic equator, a feature commonly known as the equatorial ionization anomaly (EIA). Therefore, over the low-latitude zones, the signal degradation may be more likely because of large variations of TEC near the crest of EIA owing to very large background TEC values. The temporal and spatial features of TEC at the equatorial and low latitudes are known to exhibit variability, which depends on time of the day, season, and solar activity [Galav *et al.*, 2010; Kumar and Singh, 2009]. The plasma transport which is initiated by the vertical $E \times B$ drift at the equator plays an important role in controlling the ionospheric dynamics at low latitudes. The electrostatic field which is generated by the E region dynamo gets mapped onto the F region along the magnetic lines of force. This field is the main driving force of a narrow band of enhanced eastward current known as the equatorial electrojet (EEJ). The EEJ flows in 100–120 km altitude region within $\pm 3^\circ$ latitude of the dip equator [Acharya *et al.*, 2010]. The variation of the E region dynamo electric field results in variation of the EEJ, which results in day-to-day variability of the equatorial anomaly.

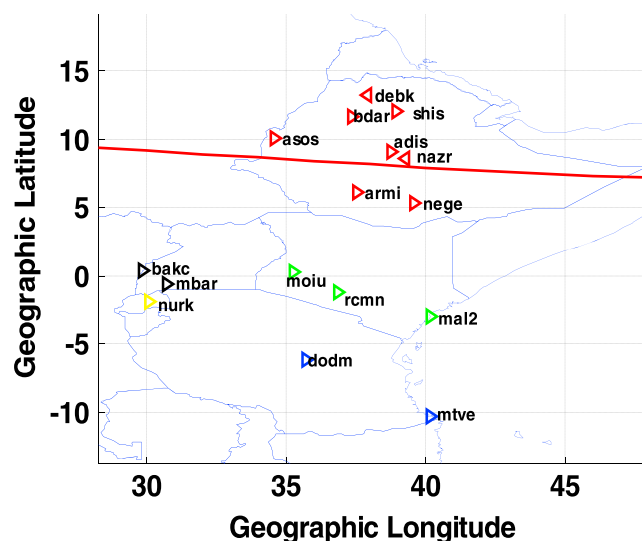


Figure 1. Map of East African region showing locations of GPS receiving stations under UNAVCO network. The red line is the magnetic dip equator.

of ionospheric data. However, with the increased access to data from the International GNSS Services (IGS) and other data inventories such as the University Navstar Consortium (UNAVCO) network, the ionospheric research over the African sector is currently on the rise. For example, previous studies on ionospheric TEC over the Kenya region [Olowendo *et al.*, 2012] have shown some significant diurnal, monthly, and seasonal trends in ionospheric variations. The occurrence of the ionospheric disturbance dynamo associated with geomagnetic storms and how it affects the evolution of the EIA has also been investigated over the East African region [Olowendo *et al.*, 2015]. Other ionospheric studies in this region include Ngwira *et al.* [2013]. However, because of the limited data and the small numbers of stations involved in such studies, the studies were not comprehensive on the role played by the equatorial anomaly on the level of ionospheric ionization over the East African region. In this work we extend the data set to 12 stations to study the dynamics of the EIA for the year 2012. A further investigation has been carried to study the ionospheric response to strong geomagnetic storm of March 2015 over the East Africa. This particular investigation has unique peculiarities since it is one of the largest storms to occur in the recent times since 2005. We believe that the results presented in this paper are necessary because they offer for the first time the possibility of studying the EIA formation, locations, and annual variations around the East African sector, which is at close proximity to the dip equator and also ionospheric response to geomagnetic storm over the region. And, as part of the studies in global ionospheric characteristics, these results will complement the ongoing studies to establish a more accurate model of the ionosphere or a basis for verifying the classical ionospheric models.

2. Data and Method of Analysis

The data used for this research were obtained from the IGS receivers at 12 locations over the East African region for the period 2012 using identical dual-frequency GPS receivers which form part of the University Navstar Consortium (UNAVCO) network (see details of the citations in the section after reference). Figure 1 shows a map of the East African countries with locations of the GPS receivers over the region. The receiver-independent exchange (RINEX) observation files obtained from the IGS website (<http://igsceb.jpl.nasa.gov/>) were processed by the GPS-TEC analysis application software, developed by Gopi Seemala [Seemala and Valladares, 2011; Ma and Maruyama, 2003]. The TEC analysis software uses the phase and code values for both L1 and L2 GPS frequencies to eliminate the effect of clock errors and tropospheric water vapor to calculate relative values of slant TEC [Sardon and Zarraoa, 1997; Sardon *et al.*, 1994; Arikani *et al.*, 2008]. Then the absolute values of TEC are obtained by including the differential code biases at the satellites which are published by the University of Bern and the receiver bias which is calculated by minimizing the TEC variability between 02:00 and 06:00 LT [Valladares *et al.*, 2009]. In the presence of the EIA, there occurs a large spatio-temporal gradient in TEC which poses a great challenge on the accuracy of the TEC owing to the mapping

In the presence of well-developed EIA, the TEC varies significantly in space and time with large latitudinal as well as the altitudinal gradients. A detailed understanding on the characteristics of the ionization anomaly crests such as the strength, location, and local time of formation of the anomaly crest are essential to understanding TEC variability. Ionospheric parameters in the anomaly region have been extensively studied particularly in the South American region, where there is dense network of Global Navigation Satellite Systems (GNSS) receivers and ionospheric observation stations [Sobral *et al.*, 2003; Batista and Abdu, 2004; Abdu *et al.*, 2006; Bertoni *et al.*, 2006]. Over the African sector there is a paucity

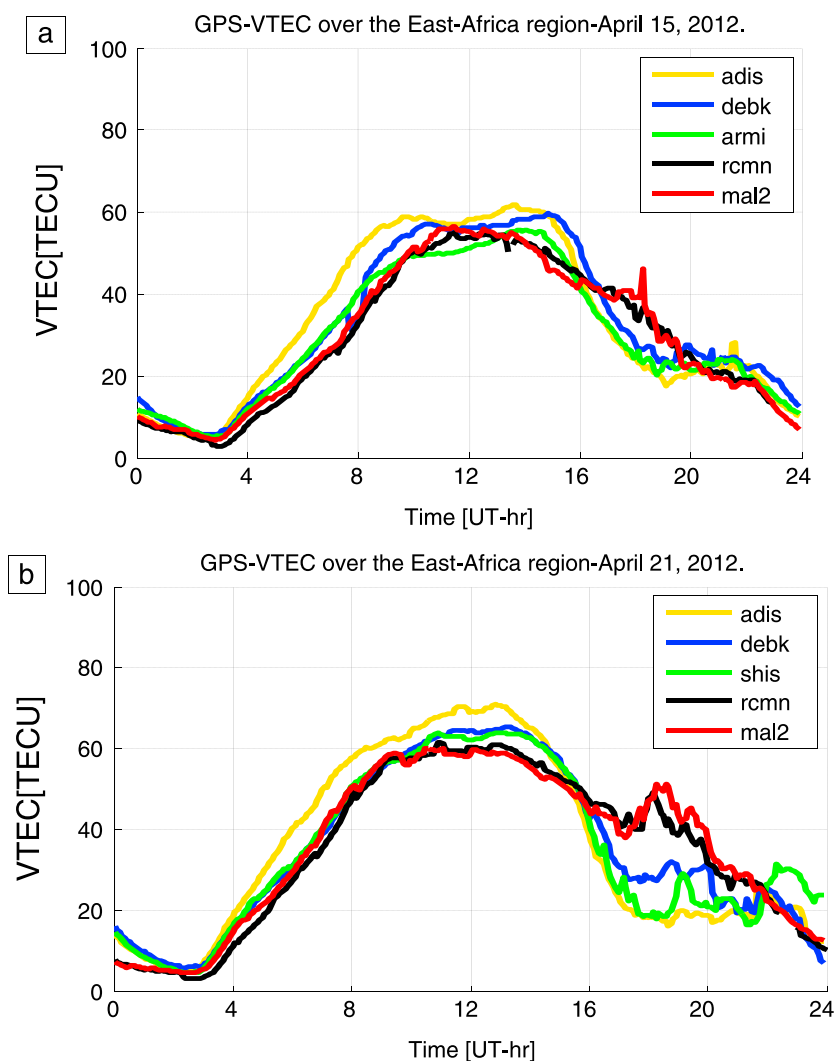


Figure 2. Diurnal variation of VTEC on (a) 15 April 2012 and (b) 21 April 2012 from five different stations located across East Africa region. The plots represent a 1 min mean VTEC computed from all the satellites in view at elevation angles above 30° at the observation stations [LT = UT + longitude/15].

function while converting the slant TEC (STEC) to vertical TEC (VTEC) at a given location within this region. To minimize this effect in the computed TEC values, an elevation threshold angle of 30° was used for all the VTEC computed. The magnetic field variation data, namely, the delta H which has been used in this work as a proxy to the daytime equatorial electrojet (EEJ), have been estimated using INTERMAGNET magnetometer and the MAGDAS magnetometer network. The pair of networks was used to help fill up the data gaps that were noticed in the INTERMAGNET network during the period of study. To achieve this, a composite data set from MAGDAS and INTERMAGNET was created to cater for days that were missing. This approach was valid given that magnetic perturbations in H from MAGDAS and INTERMAGNET correlate very well (R is 0.9996). In this approach simply, the MAGDAS H was normalized to the INTERMAGNET H , and whenever the INTERMAGNET data were missing, the normalized H was inserted.

3. Results

3.1. Ionospheric Electrodynamic Associated with Diurnal Variation of TEC

Figures 2a and 2b depict a typical diurnal variation of VTEC from five different stations as observed on 15 and 21 April 2012, respectively. The choice of the data depicts the daily formation of VTEC peaks at the region. There occurs either a double-peak formation around midday local time for the stations at the dip equator

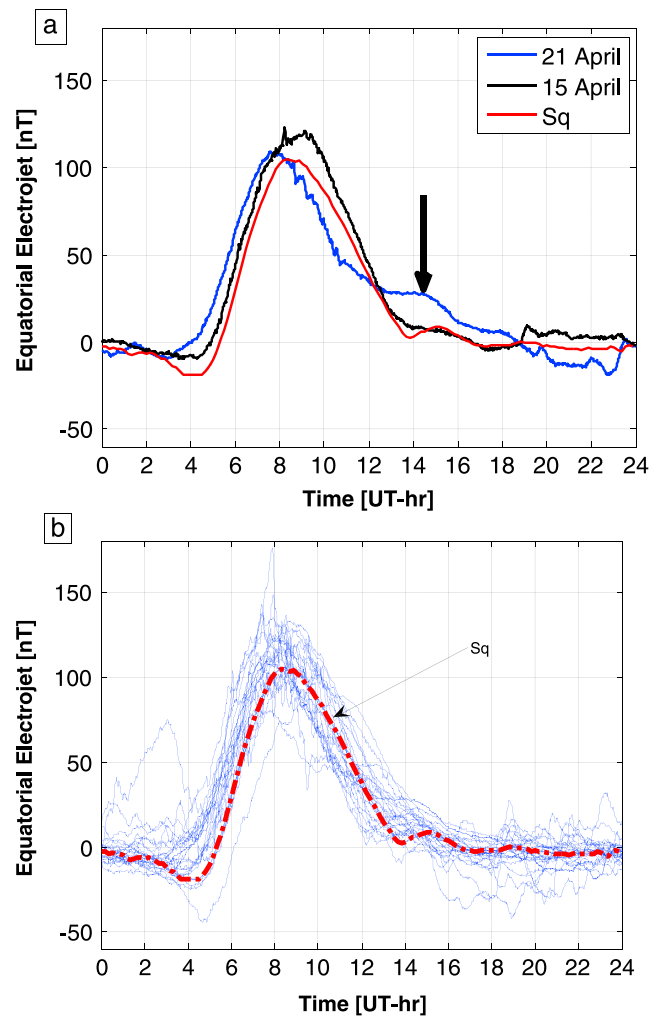


Figure 3. (a) Equatorial electrojet (EEJ) variations for 15 and 21 April 2012. The S_q values in red line are computed from the average of five quiet days in the month. The arrow indicates an increase in magnetic field variations just at the sunset hours in local time over this region (i.e., after 14:00 UT (17:00 LT)). The EEJ was computed using two magnetometer stations based in Addis Ababa (0.17°N, 110.47°E geomagnetic) and in Adigat (6.0°N, 111.06°E geomagnetic). (b) Mass plot for daily variations of the equatorial electrojet for the month of April 2012. The red dotted lines denote the diurnal variation of H , which is associated with the S_q currents.

from adis and debk stations, which are at very close proximity to the dip equator as compared to the other stations depicted in Figure 2a.

In Figures 3a and 3b, we show the variations in equatorial electrojet (EEJ) for the dates 15 and 21 April. As evident from Figure 3a, the maximum peak in EEJ variations occurred on 15 April at about 9:00 UT at an hour later than the 21 April peak, which occurred just before 08:00 UT with a much less peak in comparison to the observation on 15 April.

Studies in the measurement of average vertical plasma drifts at Jicamarca station have shown that the vertical drift velocity during the daytime is upward and has a broad peak around 11:00 LT [Fejer et al., 1991]. Taking into consideration that around midday, the ionosphere is expected to be nearly at a dynamic equilibrium in regard to ion production by solar radiation and losses by recombination, it is thus expected that the vertical plasma drift should lead to up and away movements of electrons at the magnetic equator. Such a situation should favor the formation of a maximum electron density before midday and a minimum

(like adis and debk) as shown in Figure 2a or a single-peak formation for both stations at the dip equator and those away from the dip equator as shown in Figure 2b. For a typical day, the diurnal variation in vertical TEC consists of the buildup region at sunrise hours before 4:00 UT (which is approximately before 07:00 LT), a peak in VTEC at about 12:00 UT (15:00 LT), followed by a steady decay that lasts for 2–3 h after the sunset hours in local time. A sharp rise in vertical TEC at the sunrise is attributed to the increase in the intensity of solar radiation which increases with solar zenith angle. Studies in the measurements of height of the F peak density have also indicated that during this time interval there is a sharp rise in F layer height [Radicella and Adeniyi, 1999], which is an indication that electrons are being moved to regions of lower loss rate through recombination. The adis and debk stations however show a double peak in the diurnal variation of ionization on 14 April 2012. The TEC reaches largest values in adis and debk stations which are very close to the dip equator and lower at rcnm and mal2 stations which are to the south of the magnetic equator (refer to Figure 1). The lifting of the ionosphere to regions of low recombination loss rate at the dip equator before midday local hours explains the higher premidday peaks in TEC

Table 1. Geographical Latitudes and Geomagnetic Latitudes for Receivers over the East Africa Region Used in This Study

Station Code	Geographic Longitude (°E)	Geographic Latitude (deg)	Geomagnetic Latitude
mal2	40.2	−2.9	6.61°S
moiu	35.3	0.3	2.69°S
rcmn	36.9	−1.2	4.41°S
mbar	30.7	−0.6	2.81°S
dodm	35.7	−6.2	9.12°S
adis	38.8	9.0	5.28°N
nurk	30.1	−1.9	3.98°S
asos	34.5	10.1	6.99°N
debk	37.9	13.2	9.50°N
shis	38.9	11.9	8.18°N
nege	39.6	5.3	1.57°N
mtve	40.2	−10.3	13.82°S

sometime around midday. This situation is favorable for the formation of a pre-noon peak in vertical TEC as observed in adis station in Figure 2a. The postmidday minimum in TEC is an indication that after some time the peak velocity in upward drift takes a downward trend and gets to a minimum before sunset when production of ionization is still occurring; such a situation favors the formation of postnoon peak. The absence in postnoon peak in Figure 2b for adis station indicates that the depletion of ions between midday and sunset is not reduced as fast as is in the case of Figure 2a. The ionization

peaks at the adis station will thus depend on the time of maximum electric fields, the time taken for vertical drifts and the diffusion time for electrons once lifted. Therefore, an early $E \times B$ drift like on 21 April, which gets to a maximum value around midday, does reproduce a double-humped ionization, and a later drift after midday local time may not reproduce double-humped ionization.

Our observation in Figure 2b shows that there is a decrease in postsunset peak in TEC from stations at the magnetic equator such as adis but much higher values for mal2 and rcmn, which are located away from the dip equator (refer to Table 1 for the geographical coordinates of the stations). This observation has been shown in more detailed observation by comparing a daily TEC observations for 3 months from the two stations, namely, at the dip equator (adis) and a station slightly away from the dip equator in Figure 4. The postsunset enhancement in TEC from stations away from the dip equator and the depletions in TEC at postsunset from the station at the dip equator are highly variable. As demonstrated in Figure 4 using mass plots of daily TEC for the months of February, March, and May, the postsunset peak in TEC has a day-to-day variability.

The station at the dip equator (adis) shows a small variation in day-to-day peaks in TEC after 15:00 UT and a sharp drop in TEC after this time. The contrary is the case for mal2 station, where there seems to be a large day-to-day variations in TEC after 15:00 UT. The drop in TEC is slow with an enhancement occurring at about 20:00 UT (23:00 LT), which is about 4 h after sunset local time at mal2 station.

It is therefore most likely that the high background TEC in mal2, which does not occur over adis, must be a consequence of the diffusion of the early lifted ionospheric TEC during the daytime. As seen in Figure 4 (and marked with an arrow), it is also possible that this enhancement off the station close to the equator arises from increased eastward electric fields just prior to sunset (about 14:00 UT as shown in Figure 3), which further lifts the ionosphere to higher altitudes of less recombination. We can thus deduce from this observation that the postsunset vertical plasma drift at the magnetic equator leads to spread of electrons over higher altitudes and movements away from the equator, which contributes to the drop in electron density at the station closer to the equator and an enhancement to those away such as at the mal2 and rcmn stations. Since the electrojet strength around the postsunset hours is equally highly variable, the postsunset TEC is also expected to be very variable on day-to-day basis as depicted in Figure 4, which also resembles the highly variable electrojet as depicted in Figure 3b.

The illustration of ionospheric plasma structures evolution through the entire day are shown in Figure 5 using contour plots of TEC computed from all the station in the region (refer to Figure 1 for the locations of the stations). In Figure 5, the local time versus geographic latitude contour plot of TEC from all the stations have been presented to illustrate the position and occurrences of the enhancement in TEC as seen from single stations. The contour plots presented are those for the same day as in Figure 2.

As evident from Figure 5a, there are two large enhanced electron density structures between 12:00 and 16:00 LT, which appear to the south and north of the dip equator. This observation depicts a well-developed EIA crests. In Figure 5b, the large-density structure of electrons does not separate into two parts, and this indicates that the anomaly did not form. As can be observed in Figure 2b, the daily TEC on such a day does not depict a double-humped peak. It is however clear from Figure 5b that

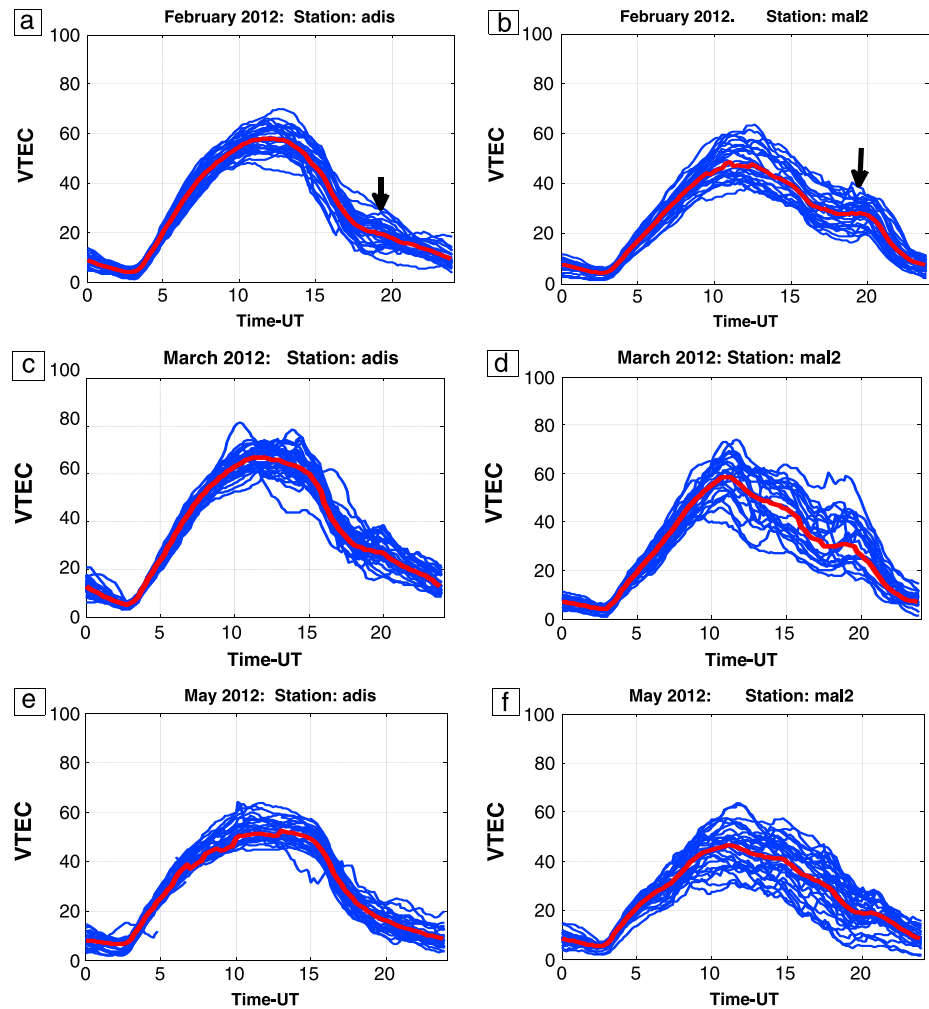


Figure 4. Monthly mass plots of the diurnal variation of the TEC for the months of February, March, and May 2012 over (a, c, and e) adis in the first column and (b, d, and f) mal2 in the second column. The red plot indicates the monthly mean diurnal TEC values. The arrow on the figures in the top indicates the decrease in TEC and an enhancement in TEC in adis and mal2, respectively.

the presence of significant large electron density structures some 2 h after the local sunset hour (~20:00 LT) does coincide with the observations of postsunset enhancement seen in Figures 2b and 4 from stations in the southern latitudes of the geomagnetic equator. From Figures 5a and 5b, it is clear that there is no symmetry in the level of ionization on a particular observation day. For instance, in Figure 5b, the large structures in electron density are more to the south than to the north, and the same is true for Figure 5a, where the southern anomaly forms much more prominently than the north, a factor which could be attributed to the fact that the northern anomaly is not well covered by data (the data extend only up to about 10°N, which is still at the dip equator), and it might not be possible to tell how well or poorly the anomaly forms to the north. The postsunset enhancement observed in TEC over the East African sector is a consequence of the interaction of the *E* and *F* region dynamo, which results into an enhancement of the eastward electric field (a phenomenon commonly referred to as the prereversal enhancement, PRE) before it turns westward at dusk. The electrojet strength therefore at the sunset hours will depend on the conductivity of equatorial ionospheric *E* region and the electric fields driving the current. As a result of the increased vertical drift caused by the PRE, the densities in the EIA are enhanced and can persist well into the evening. Therefore, the density and latitudinal extent of the nighttime EIA is strongly associated with the vertical drift velocity during the day, at dusk, and in the evening hours.

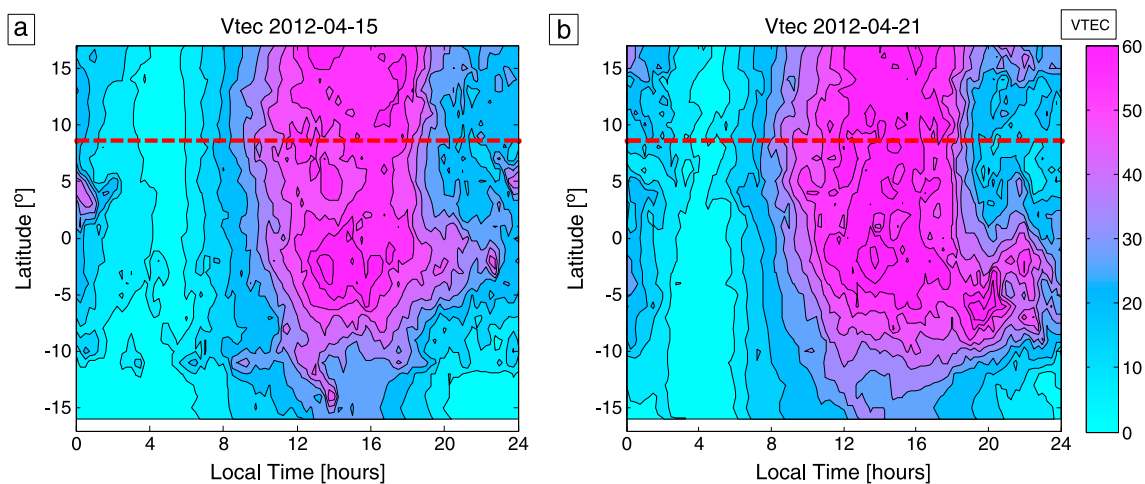


Figure 5. (a and b) Plot of VTEC showing variations with the local time and latitudes of IPPs. The red dashed line shows the mean location of the geomagnetic equator over the region covered by the IPPs.

3.2. Annual Variations in EIA over the East African Sector

The evolution and formation of the ionization anomaly over the East Africa sector for the year 2012 is illustrated in Figure 6, which shows the monthly mean diurnal local time versus geographic latitude contours side by side for all the months.

From Figure 6, the occurrence of the anomaly crest of the EIA is between 13:00 LT and 15:00 LT. The occurrence of the crests depicts two peaks spreading over the various latitudes. The high density of TEC above the mean position of the magnetic equator which has been marked with a yellow line in the Figure 6 appears much stronger and broader than that which forms to the south of the magnetic equator. The high intensity of the TEC at the dip equator is an indication on the lifting of the ionospheric *F* layer by a rather weaker upward momentum that does not enable movement of lifted plasma away from the equator and hence leading to no crest formation at later hours of the day. The formation of the anomaly crest depicts a seasonal trend, whereby the crest is stronger with a longer latitudinal spread during the equinox months and weakest in the solstices. There is however asymmetry in the equinoxes, whereby the September and October crest has well-developed double crest than the March and April crest. The trends depicted by the seasonal variation in the EIA formations are similar to those that had previously been seen in seasonal variation in TEC over this region [for example in *Tariku, 2015; Amabayo et al., 2014; Olwendo et al., 2012*]. It has been shown that the TEC trends also does correlate well with the solar activity indices such as the sunspot and *F*_{10.7} indices [*Gupta and Singh, 2001; Bagiya et al., 2009; Chen et al., 2009; Galav et al., 2010; Liu et al., 2013*]. The formation of the EIA is strongly dependent on the solar activity levels and is expected to weaken during the low solar activity cycle. During the year 2012, there was a great increase in the mean annual sunspot number, which rose to 84.5 from 80.5 in the year 2011. We attribute the well-formed southern anomaly crest during the equinoxes to the abundance photoelectrons due to the fact that the latitudes for the midday overhead Sun occur in the region near the magnetic equator. Combined with the expectedly large eastward electrojet leads to well-developed fountain effect, which is associated with the well-formed EIA crest later in the day in the latitudes away from the dip equator.

3.3. Geomagnetic Storm Effect on EIA Formation over the East African Region: A Case Study

In this section we look at a case study on how geomagnetic storm affects the EIA anomaly formation at the low-latitude regions over the East African sector. Our previous study on geomagnetic storms over this region have shown the occurrence of TEC enhancements during the recovery phase of the storm and also an increase in intensity of the amplitude and latitudinal extent of the EIA during the recovery phase of the storm. Both features were attributed to ionospheric disturbance dynamo electric fields during the recovery phase of the storm, which in turn does modify the equatorial fountain effect [*Olwendo et al., 2015*]. This case study presents a unique space weather event that was observed on 17 March 2015 and presents one of the largest storms in the recent times since 2005.

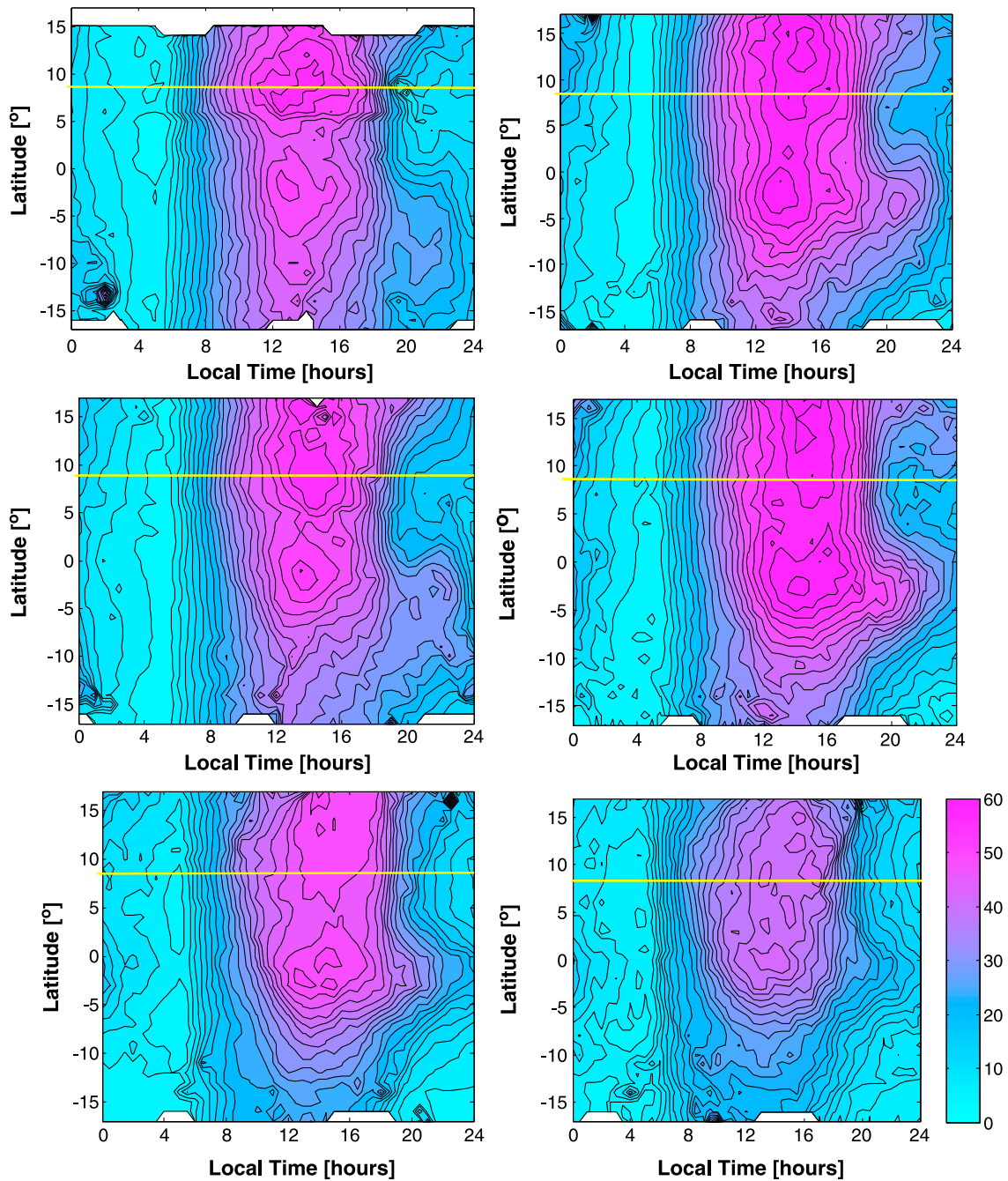


Figure 6. (a) VTEC distribution versus time of day and latitude in terms of monthly mean values for 2012 for all 12 GPS receivers. The data were binned in 0.25 h increments and latitude increments of 1°. The yellow line shows the mean location of the geomagnetic equator over the region covered by the IPPs. The first column represents the January, March, and May months, while the second column represents the months of February, April, and June, respectively. (b) Same as in Figure 6a but for the months of July, September, and November in column 1 and August, October, and December in column 2.

The solar wind parameters used for the analysis of this geomagnetic storm were obtained from the Advanced Composition Explorer satellite data, which are available and maintained by the Coordinated Data Analysis Web (CDAWeb) in the website <http://omniweb.gsfc.nasa.gov/>, and a high-resolution data of 5 min averages were used in this study. Figures 7a and 7b show the measurements of the magnetic interplanetary conditions for the period of 16–20 March 2015.

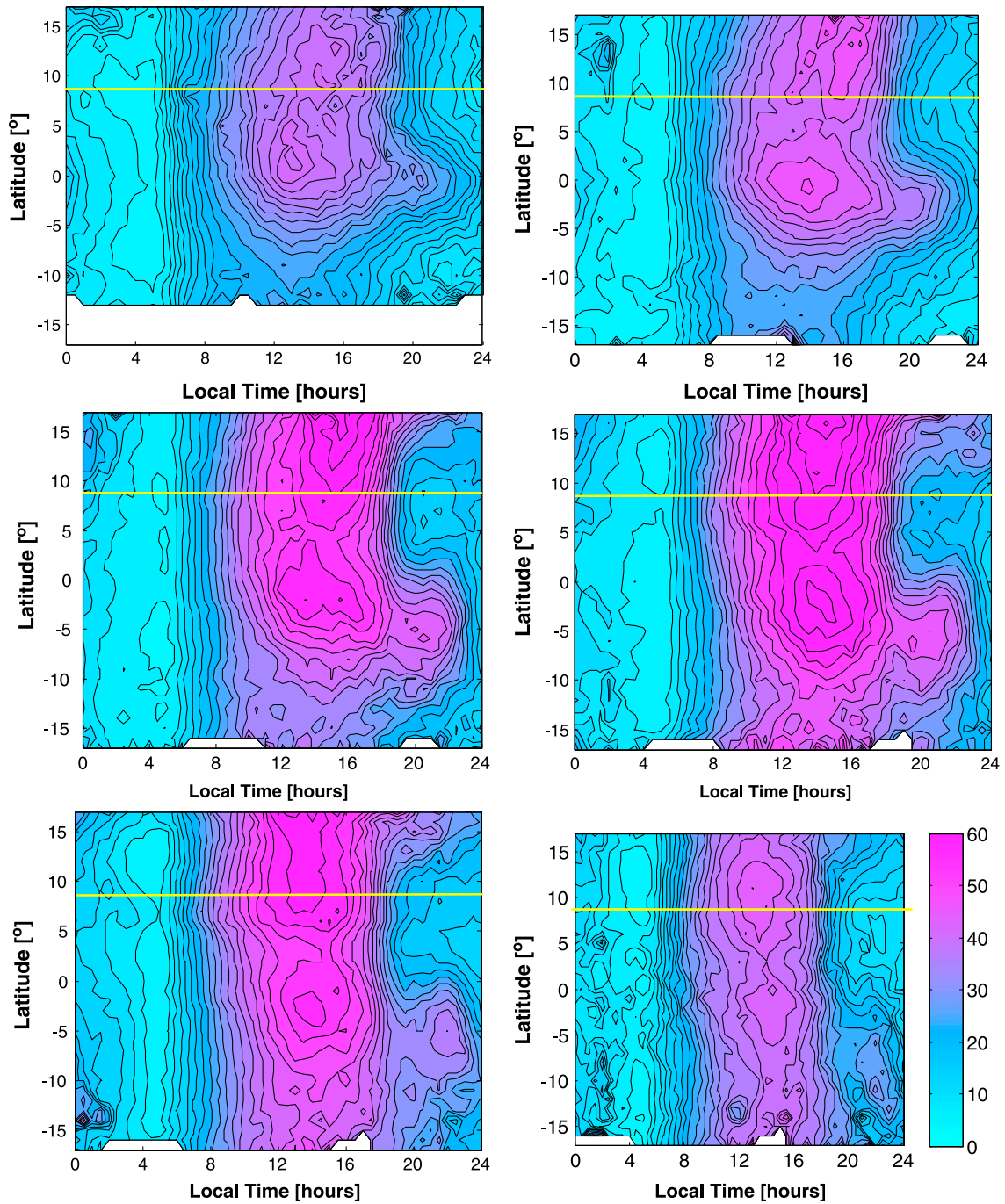


Figure 6. (continued)

Figure 7a reveals that the storm commencement started on 17 March at ~04:00 UT. The onset of the storm was marked by a rapid increase in the solar wind speed from 400 km/s to ~500 km/s at 06:00 UT. The interplanetary magnetic field (IMF) B_z turned southward at exactly 06:00 UT, which also coincided with the onset of the main phase of the storm. Three hours later there was a sharp northward turning of the IMF B_z at about 09:00 UT that resulted into a short recovery phase between 09:00 and 12:00 UT. The *SYM-H* started a strong negative excursion after 12:00 UT for the next 12 h to attain a minimum value of over -200 nT just at the end of 17 March (24:00 UT). The short-lived sharp turning of the IMF B_z northward did occur at the same time when the interplanetary electric fields (IEF_y) showed a

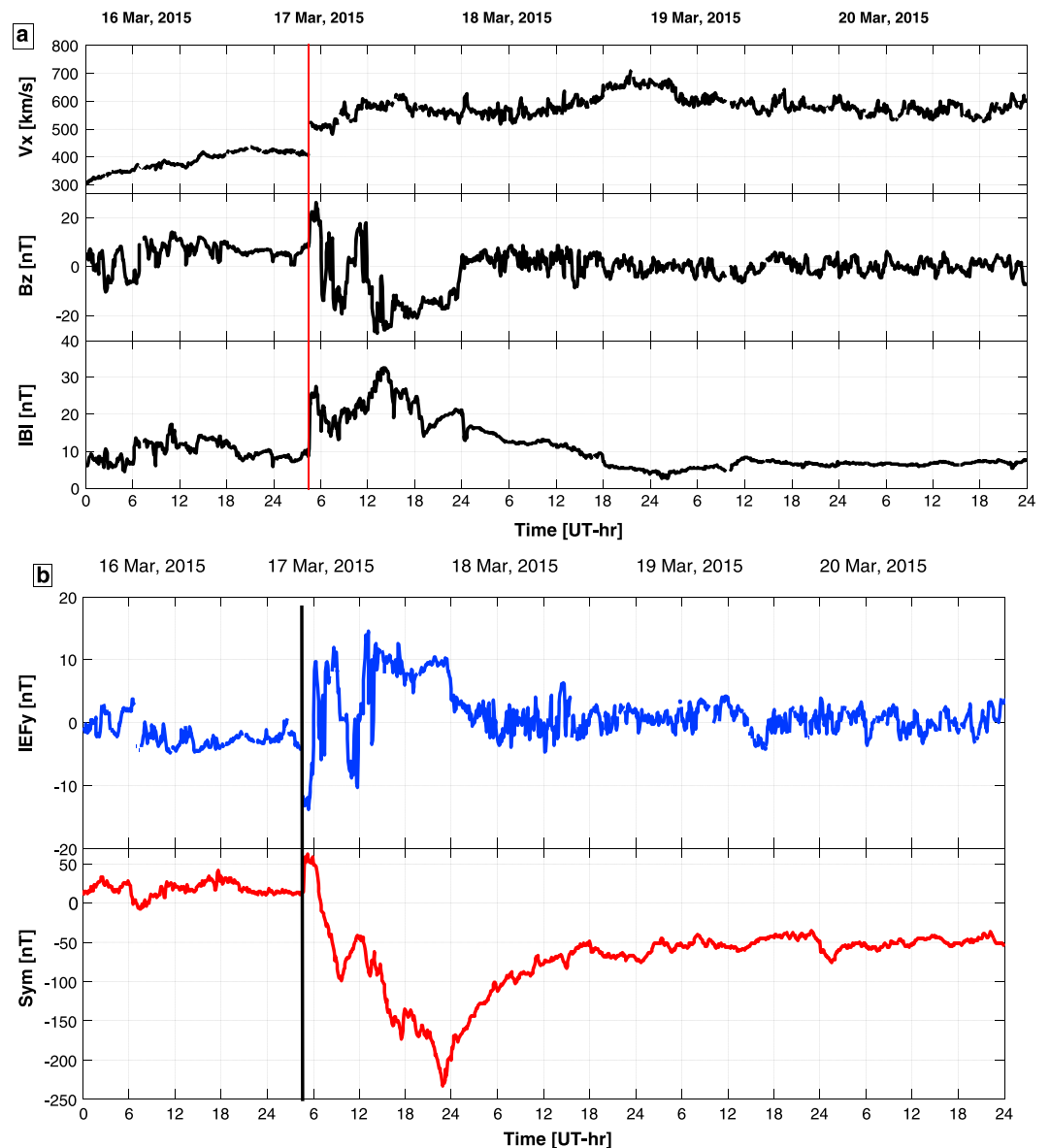


Figure 7. (a) Variations of solar wind speed V_x , IMF B_z , and average magnetic field $|B|$ and (b) variations of IMF B_z , interplanetary magnetic field E_y and SYM-H for the period of 16–20 March 2015. The red and black lines show the commencement of the storm on 17 March 2015.

reduction over the same time. The IMF B_z started turning northward by 12:00 UT on 17 March with the IEF_y getting to a constant value over the same period.

The recovery phase of the storm began gradually from 18 March at 00:00 UT to 20 March. The magnetic disturbance observed from the magnetic observation station based in Addis Ababa (Ethiopia) over the same period is shown in Figure 8. The sharp B_z turning northward on 17 March did coincide with a very strong counterelectrojet between 09:00 and 12:00 UT as evident from Figure 8. The EEJ recovered to zero levels sometimes after 12:00 UT but remained disturbed for the rest of the day. The effect of the storm showed a suppressed EEJ during the recovery phase, which is consistent with the statistical results from the Peruvian and Indian sectors presented by Yamazaki and Kosch [2015]. The EEJ regained its levels prior to the storm at the end of the recovery phase of the storm on 21 March.

The response to ionospheric TEC from four different stations in the East Africa sector is illustrated in Figure 9. Due to inadequate data from most of the stations during this period it was not possible to generate contour

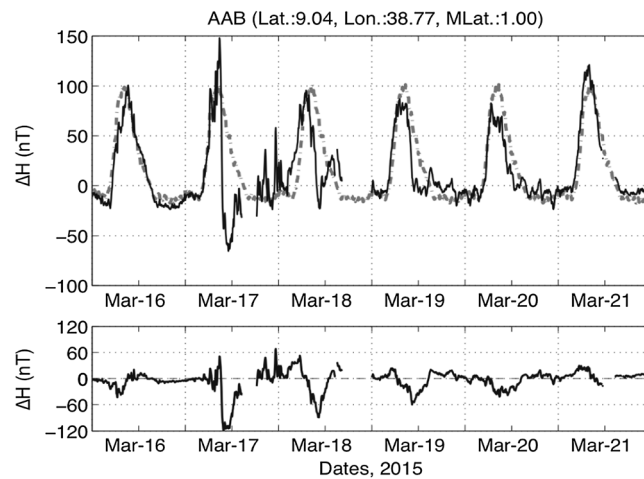


Figure 8. Variations of the H component of the Earth's magnetic field observed at Addis Ababa (AAB) for the period of 16 to 21 March 2015. (top) The solid line is the H component geomagnetic field minus the $SYM-H$, while the dotted line represents the monthly median daily variations, i.e., the monthly median at each time of the day. The zero level is defined as the median value of the month. (bottom) The difference between the observed and the monthly median daily variations.

plots over the region to monitor EIA formation during the storm. In each plot, the TEC observation during the storm and the monthly median values of TEC are presented alongside the corresponding deviation in TEC (ΔTEC). The deviations in TEC are obtained by subtracting the corresponding values of the median from the values of TEC during the storm. The negative deviation from the corresponding monthly median values of TEC for the period of 18–20 March, the stations located away from the dip equator (mal2, moi, and mbar) do show a negative storm effect, while the positive deviations in TEC at adis station do show positive storm effect for the same period. The counter EIJ on 17 March caused significant TEC depletions from the adis station. The adis station being

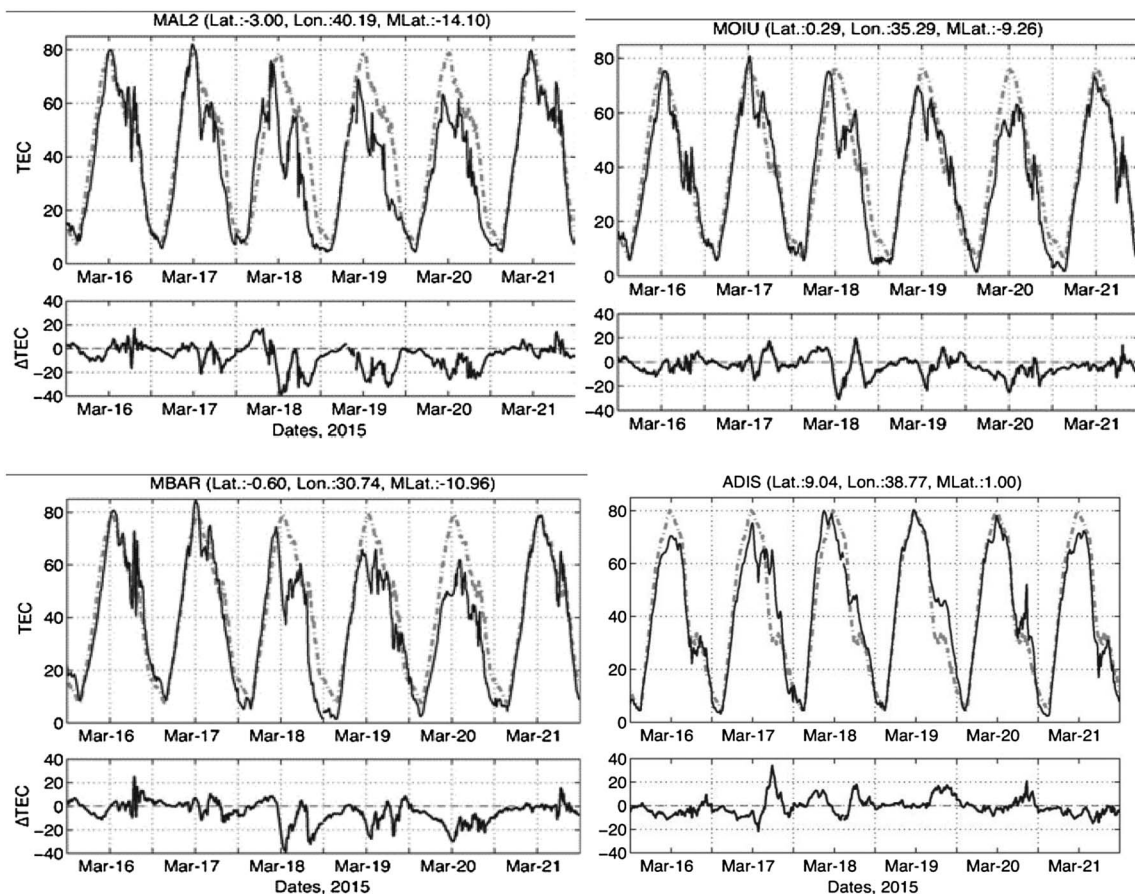


Figure 9. Ionospheric TEC response to geomagnetic event during the period of 16 to 21 March 2015 from stations within the East African sector: (top) adis, (middle) mal2, and (bottom) mbar.

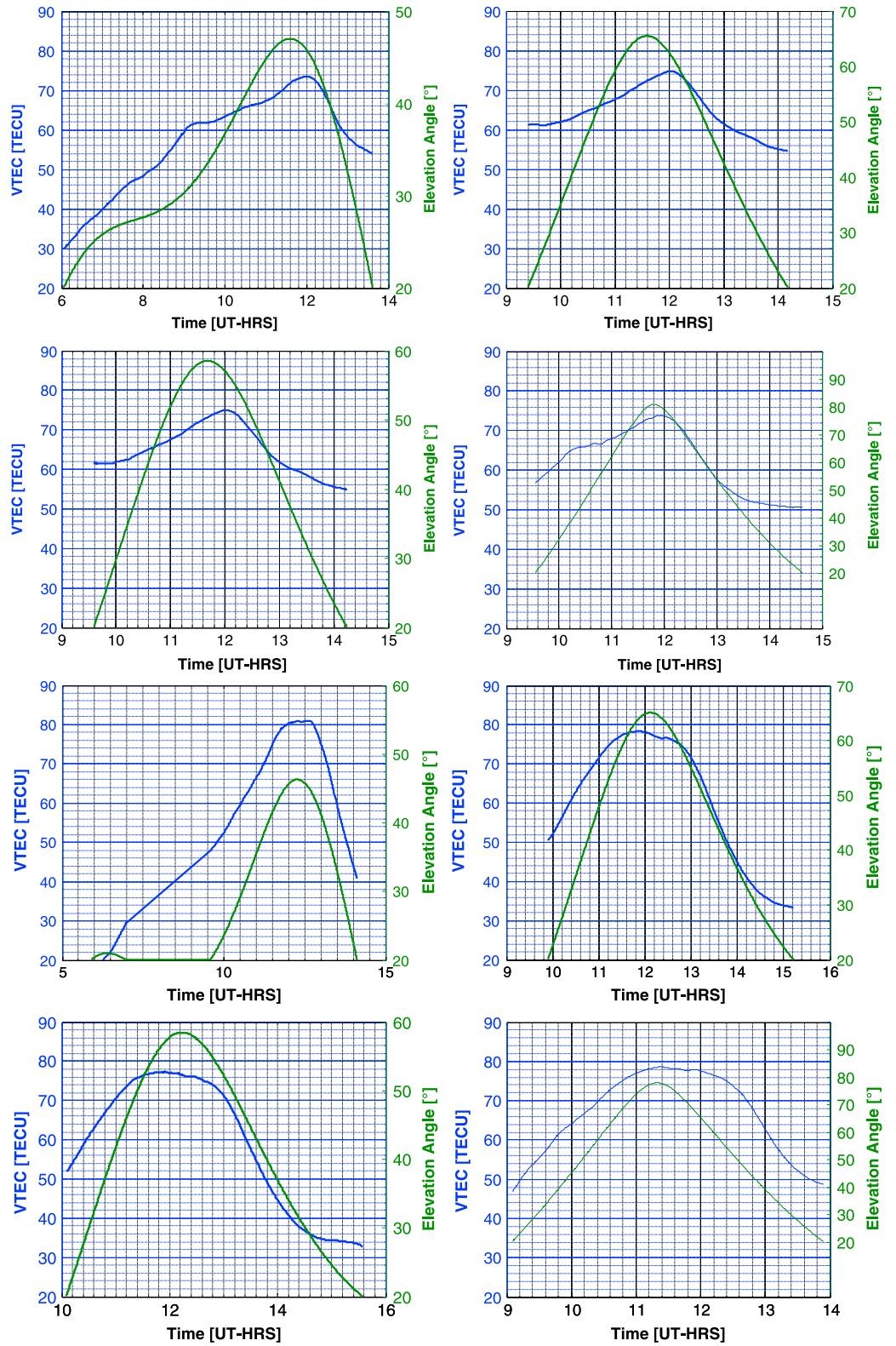


Figure 10

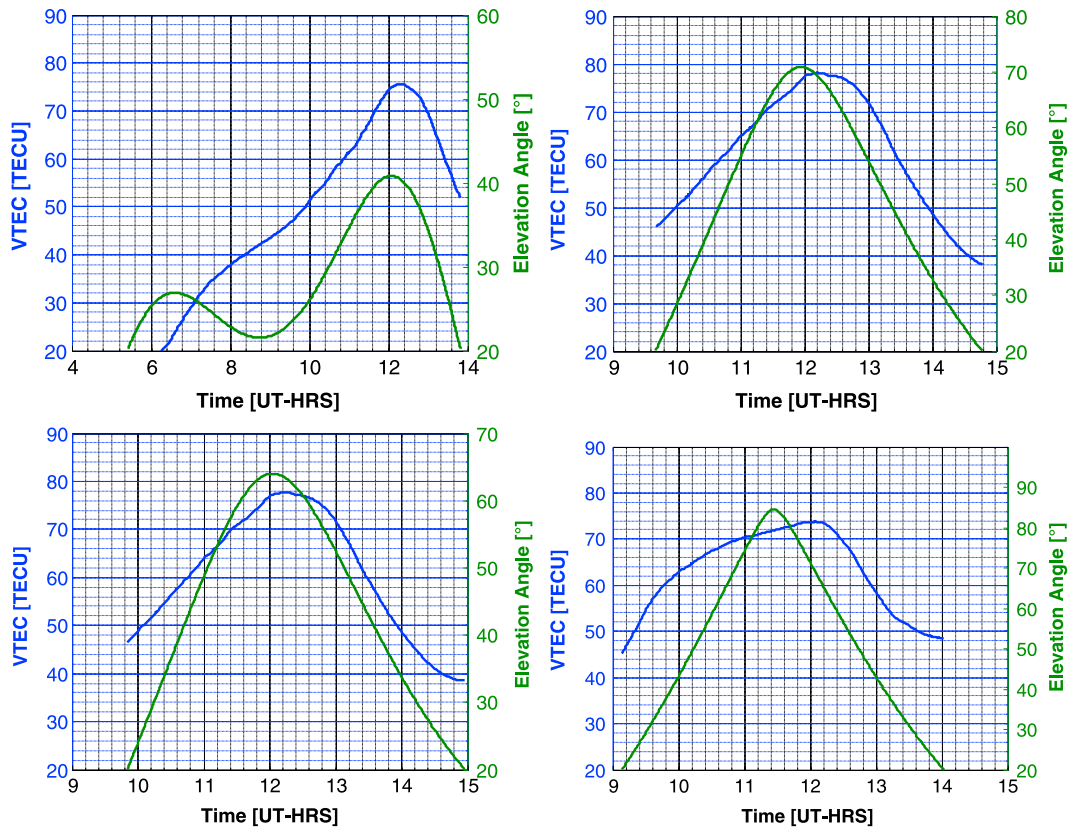


Figure 10. (continued)

at the dip equator is expected to show TEC depletions due to the counter EEJ, which suppresses the fountain formation. It is however evident that the effect of the counter EEJ as felt by the stations away from the dip equator such as mal2, moi, and mbar showed a slight enhancement in TEC on 17 March. The enhancement in TEC as observed on 17 March from stations away from the equator is rather unique since the suppression of the fountain formation is also expected to affect the TEC peaks from the stations at the ionization anomaly crests such as the three indicated in this study. A more detailed behavior of TEC has been presented in Figures 10a–10c by identifying the individual satellites (PRN) that were visible from the station during the period when there were depletions at the adis station and enhancement at the stations away from the dip equator.

Our previous study on the ionospheric response to magnetic storms over this region had shown that during geomagnetic storm, the EIA formation get modified by either being suppressed by a counter electrojet (CEJ) arising from the northern turning of the IMF B_z fields or enhanced by prompt penetration of magnetospheric electric fields associated with the IMF B_z turning southward and also ionospheric disturbance dynamo electric fields that are raised during the quiet time storm conditions [Olwendo *et al.*, 2015]. In Figure 10, the ionospheric response on 17 March at the onset of the storm is characterized by (1) a steep density drop at the adis station at the dip equator starting 12:00 UT and (2) a sudden enhancement in the ionization density from stations away from the dip equator starting 12:00 UT. The steep density drop at the adis is rather expected, and this can be attributed to the CEJ that occurred between 9:00 and 12:00 UT that prompted a downward

Figure 10. (a) Observations of vertical TEC related to satellites with (row 1) PRNs 9 and 10 and (row 2) 20 and 28 in row 2, respectively, over adis station on 17 March 2015. All the satellites show gradual decrease in TEC at 12:00 UT. (b) Observations of vertical TEC related to satellites with (row 1) PRNs 9 and 10 and (row 2) 20 and 28, respectively, over mal2 station on 17 March 2015. The TEC observation around 12:00 UT does show a constant high TEC values lasting till 13:00 before a slow decrease. (c) Observations of vertical TEC related to satellites with (row 1) PRNs 9 and 10 and (row 2) 20 and 28, respectively, over moi station on 17 March 2015. The TEC observations around 12:00 till 13:00 UT show the enhancement for all the satellites except PRN 28, which shows a sharp decrease in TEC from 12:00 UT.

movement of the raised F region to lower altitudes. We attribute the enhanced electron density at about 12:00 UT at stations away from the equator to the presence of TEC at higher latitudes, which had been initiated by the early formation of the fountain effect prior to the arrival of the magnetospheric electric fields that caused a strong CEJ between 9:00 and 12:00 UT. For the adis station daily TEC gained to nearly normal values from 18 to 20 March unlike the other stations which showed a very strong negative storms effect during the same period. While it is expected that after the storm, once the EEJ returns to its value prior to the storm, the daily peaks in TEC should also regain in all the stations within proximity, it was not the case in this observation. There was a strong negative storm effect in TEC from stations away from the dip equator, while at the dip equator TEC values regained to the values prior to the storm. We speculate the negative storm effect evident from the three stations away from the equator to changes in ion composition in the thermosphere occasioned by the storm. It is known that during storms, there occurs the expansion of neutral atmosphere due to heating at the high latitudes. The expanding neutral atmosphere results in the upwelling which increases the mean molecular mass in the thermosphere. The expansion also results into pressure gradients which modify the global thermospheric circulation and due to the enhanced equatorward winds; composition changes are transported to the low latitudes where they modify the F regions [Buonsanto, 1999; Abdu *et al.*, 1991]. Depending upon the intensity of a storm the disturbance in the composition could modify the equatorial thermosphere to produce a negative disturbance in ionospheric electron densities [Abdu *et al.*, 1991]. Because the chemical loss rate decreases exponentially with height, the negative effects are more expected when the F layer peak is situated at lower heights. With reference to our stations of observation, we expect that the F layer over the adis station is higher than the other stations (at the anomaly crest) since it is right over the equator. Therefore, it is expected that any thermospheric composition effect would produce significantly a more negative disturbance at the moiu, mal2, and mbar stations, which are situated at the anomaly crest. Also, if this is coupled with a possibility of an equatorward decrease of the thermospheric disturbance effects, then the significance of an expected negative disturbance in the electron density over the equator could be diminished for most of the storms [Abdu *et al.*, 1991].

4. Discussion and Conclusion

In this work the diurnal and annual variations of the vertical total electron content (TEC) derived from up to 12 IGS GPS receiver stations over the East African region have been presented. A case study on the storm of 17 March 2015 has also been analyzed. The daily maximum TEC value around the East Africa sector occurs in the stations around the 10°N (adis and debk in Ethiopia). The stations located to the south of the magnetic equator show lower values of the TEC peaks compared to those in the northern part. This feature is also reflected in the location and formation of the crest of the EIA. The TEC has larger values over the geomagnetic equator than at the crest on this particular day. The diurnal variation in TEC as shown in Figures 2 and 4 depicts an enhancement in TEC after local sunset hours, a feature which greatly depends on the strength of the equatorial ionization anomaly, which has seasonal, solar activity, and geomagnetic activities and latitudinal dependence [Bagiya *et al.*, 2009]. The daily peak TEC value of the crest reveals both seasonal and semiannual variations; the peak TEC values and a well-developed crest occur in the equinoxes, while a weak crest forms in the solstices. During the equinoxes the subsolar point is near the equator, where the eastward electric field is often larger, and this intensifies the fountain effect which controls ionization levels at the equator. In solstices the subsolar point moves to higher latitudes, and the fountain is expected to wane, and hence, the reduced ionization peaks in the solstices. The transequatorial winds also changes the recombination rate by lifting the ionospheric height on either side of the equator and hence increasing or decreasing the electron density. Our results in this work have indicated the effect of $E \times B$ force on the plasma dynamics in this region as a key factor influencing the ionization levels. Vertical plasma drift measurements taken at Jicamarca which is an equatorial station over a long period of time showed that the daytime magnitudes are highest during the equinox months (March-April and September-October) [Fejer *et al.*, 1991]. We therefore attribute the well-formed EIA crests during the months of March, April, September, and October to the high vertical plasma drift associated with the equinoxes. And, the occurrence of postnoon peak is favorable when the daytime upward plasma drift velocity attains a maximum earlier and also begins to decrease earlier; under this condition plus the fact that the source of ion production is still present during the day time does favor the development of a more prominent postnoon peak at anytime. During the equinoxes since the subsolar point is much closer to the geomagnetic equator, this equally results in different types of transequatorial winds at the EIA region which

might accelerate the formation of the anomaly. This behavior is depicted in annual variations in the crest formations presented in this investigation.

A global-scale study on ionospheric variations have indicated that there exists a close coupling between hemispheres and therefore suggest a key role of the dynamic and electrodynamical processes in the ionospheric semiannual variation [Ma *et al.*, 2003; Liu *et al.*, 2009]. For instance, Ma *et al.* [2003] proposed that the semiannual variation in the ionosphere at low latitude could be due to the diurnal tide that modulates the variations of equatorial electric fields and equatorial electrojet via the wind dynamo processes and further control the ionosphere through the fountain effect. The complex coupling of the magnetosphere-thermosphere-ionosphere over the low-latitude region is yet to be well understood, given that there is still a large gap in database over a longer period. The case study on the storm on 17 March has been characterized by very strong negative effect during the recovery phase of the storm as observed from station away from the dip equator. We have suggested the cause of the negative storm effect to the thermospheric composition disturbance generated by the energy depositions during the storm. We however need to point out that there is still a great need of relevant data collection in measurements of thermospheric-ionosphere coupling electrodynamic drivers such as wind, temperature, and composition changes.

Acknowledgments

I wish to thank the Atlantic Radio Science, AT-RASC, organizers for supporting one of the authors (Olwendo Joseph) in his participation in the AT-RASC conference as a recipient of the Young Scientist Award. The authors would also like to thank the University Navstar Consortium (UNAVCO) and the Coordinated Data Analysis Web (CDAWeb) for allowing access to their websites for GPS data and solar wind magnetic parameters, respectively. We appreciate the Geophysical Observatory of Addis Ababa University and INTERMAGNET and MAGDAS for providing the magnetic field data and for promoting high standards of magnetic observatory practice. We also thank Gopi Krishna Seemala for providing access to the GPS-TEC analysis software used in this work.

References

- Abdu, M. A., J. H. A. Sobral, E. R. Paula, and I. S. Batista (1991), Magnetospheric disturbance effects on the equatorial ionization anomaly (EIA): An overview, *J. Atmos. Terr. Phys.*, *53*, 757–771.
- Abdu, M. A., I. S. Batista, B. W. Reinisch, J. H. A. Sobral, and A. J. Carrasco (2006), Equatorial *F* region evening vertical drift and peak height, during southern winter months: A comparison of observational data with the IRI descriptions, *Adv. Space Res.*, *37*, 1007–1017.
- Acharya, R., B. Roy, M. R. Sivaraman, and A. Dasgupta (2010), An empirical relation of daytime equatorial total electron content with equatorial electrojet in the Indian zone, *J. Atmos. Sol. Terr. Phys.*, *72*, 774–780.
- Amabayo, E. B., E. Jurua, P. J. Cilliers, and J. B. Habarulema (2014), Climatology of ionospheric scintillation and TEC trend over the Ugandan region, *Adv. Space Res.*, *53*, 734–743.
- Arikan, F., H. Nayir, U. Sezen, and O. Arikan (2008), Estimation of single station interfrequency receiver bias using GPS-TEC, *Radio Sci.*, *43*, RS4004, doi:10.1029/2007RS003785.
- Bagiya, M. S., H. P. Joshi, K. N. Iyer, M. Aggarwal, S. Raviridran, and B. M. Pathan (2009), TEC variations during low solar activity period (2005–2007) near the equatorial ionospheric anomaly crest region in India, *Ann. Geophys.*, *27*, 1047–1057.
- Batista, I. S., and M. A. Abdu (2004), Ionospheric variability at Brazilian low and equatorial latitudes: Comparison between observation and IRI model, *Adv. Space Res.*, *34*, 1894–1900.
- Bertoni, F., Y. Sahai, W. L. C. Lima, P. R. Fagundes, V. G. Pillat, F. Becker-Guedes, and J. R. Abalde (2006), IRI-2001 model predictions compared with ionospheric data observed at Brazilian low latitude stations, *Ann. Geophys.*, *24*, 2191–2200.
- Buonsanto, M. J. (1999), Ionospheric storms—A review, *Space Sci. Rev.*, *88*, 563–601.
- Chen, Y., L. Liu, W. Wan, X. Yue, and S.-Y. Su (2009), Solar activity dependence of the topside ionosphere at low latitudes, *J. Geophys. Res.*, *114*, A08306, doi:10.1029/2008JA013957.
- Davies, K. (1990), *Ionospheric Radio*, Peter Peregrinus, London.
- Fejer, B. G., E. R. de Paula, S. A. Gonzalez, and R. F. Woodman (1991), Average vertical and zonal *F* region plasma drifts over Jicamarca, *J. Geophys. Res.*, *96*, 13,901–13,906, doi:10.1029/91JA01171.
- Galav, P., N. Dashora, S. Sharma, and R. Pandey (2010), Characterization of low latitude GPS-TEC during very low solar activity phase, *J. Atmos. Sol. Terr. Phys.*, *72*, 1309–1317.
- Garner, T. W., T. L. Gaussiran II, B. W. Tolman, R. B. Harris, R. S. Calfas, and H. Gallagher (2008), Total electron content measurements in ionospheric physics, *Adv. Space Res.*, *42*, 720–726.
- Gupta, J. K., and L. Singh (2001), Long term ionospheric electron content variations over Delhi, *Ann. Geophys.*, *18*, 1635–1644.
- Kumar, S., and A. K. Singh (2009), Variation of ionospheric total electron content in Indian low latitude region of equatorial anomaly during May 2007–April 2008, *Adv. Space Res.*, *43*, 1555–1562.
- Liu, G., W. Huang, J. Gong, and H. Shen (2013), Seasonal variability of GPS-VTEC and model during low solar activity period (2006–2007) near the equatorial ionization anomaly crest location in Chinese zone, *Adv. Space Res.*, *52*, 366–376.
- Liu, L., W. Wan, B. Ning, and M.-L. Zhang (2009), Climatology of the mean total electron content derived from GPS global ionospheric maps, *J. Geophys. Res.*, *114*, A06308, doi:10.1029/2009JA014244.
- Ma, G., and T. Maruyama (2003), Derivation of TEC and estimation of instrumental biases GEONET in Japan, *Ann. Geophys.*, *21*, 2083–2093.
- Ma, R., J. Xu, and H. Liao (2003), The features and a possible mechanism of semiannual variation in the peak electron density of the low latitude *F*₂ layer, *J. Atmos. Sol. Terr. Phys.*, *65*, 47–57, doi:10.1016/S1364-6826(02)00192-X.
- Ngwira, C. M., G. K. Seemala, and J. Bosco Habarulema (2013), Simultaneous observations of ionospheric irregularities in the African low-latitude region, *J. Atmos. Sol. Terr. Phys.*, *97*, 50–57.
- Olwendo, O. J., P. Baki, C. Mito, and P. Doherty (2012), Characterization of ionospheric GPS total electron content (GPS-TEC) in low latitude zone over the Kenyan region during a very low solar activity phase, *J. Atmos. Sol. Terr. Phys.*, *84–85*, 52–61.
- Olwendo, O. J., Y. Yamazaki, P. Cilliers, P. Baki, C. M. Ngwira, and C. Mito (2015), A study on the response of equatorial ionization anomaly over the East African Sector during the geomagnetic storm of November 13, 2012, *Adv. Space Res.*, doi:10.1016/j.asr.2015.03.011.
- Opperman, B. D. L., P. J. Cilliers, L. McKinnell, and R. Haggard (2007), Development of a regional GPS-based ionospheric TEC model for South Africa, *Adv. Space Res.*, *39*(5), 808–815, doi:10.1016/j.asr.2007.02.026.
- Prasad, S. N. V. S., P. V. S. Rama Rao, D. S. V. V. D. Prasad, K. Venkatesh, and K. Niranjana (2012), On the variabilities of the total electron content (TEC) over the Indian low latitude sector, *Adv. Space Res.*, *49*, 898–913.
- Radicella, S. M., and J. O. Adeniyi (1999), Equatorial ionospheric electron density below *F*₂ peak, *Radio Sci.*, *34*, 1153–1163, doi:10.1029/1999RS900071.

- Sardon, E., and N. Zarraoa (1997), Estimation of total electron content using GPS data: How stable are the differential satellite and receiver instrumental biases?, *Radio Sci.*, *32*, 1899–1910, doi:10.1029/97RS01457.
- Sardon, E., A. Rius, and N. Zarraoa (1994), Estimation of the transmitter and receiver differential biases and the ionospheric total electron content from global position system observation, *Radio Sci.*, *29*, 577–586, doi:10.1029/94RS00449.
- Schaer, S., W. Gurtner, and J. Feltens (1998), *IONEX: The IONosphere Map Exchange Format Version 1*, Astron. Inst., Univ. of Bern, Switzerland and Darmstadt, Germany.
- Seemala, G. K., and C. E. Valladares (2011), Statistics of total electron content depletions observed over the Southern American continent for the year 2008, *Radio Sci.*, *46*, RS5019, doi:10.1029/2011RS004722.
- Sobral, J. H. A., M. A. Abdu, P. Muralikrishna, J. W. Labelle, V. M. de Castilho, and C. J. Zamlutti (2003), Rocket and ground-based sounding versus IRI representation, *Adv. Space Res.*, *31*(3), 569–575.
- Tariku, Y. A. (2015), Patterns of GPS-TEC variations over low-latitude regions (African sector) during the deep solar minimum (2008 to 2009) and solar maximum (2012 to 2013) phases, *Earth Planets Space*, *67*, 35, doi:10.1186/s40623-015-0206-2.
- Valladares, C. E., J. Villalobos, M. A. Hei, R. Sheehan, S. Basu, E. Mackenzie, P. H. Doherty, and V. H. Rios (2009), Simultaneous observation of travelling ionospheric disturbances in the Northern and Southern Hemispheres, *Ann. Geophys.*, *27*, 1501–1508.
- Wu, C. C., C. D. Fry, K. Liou, and C. L. Tseng (2004), Annual TEC variation in the equatorial anomaly region during the solar minimum: September 1996–August 1997, *J. Atmos. Terr. Phys.*, *66*, 199–207.
- Xu, Z., W. Wang, N. Zhou, X. Song, and H. Zhu (2012), Variability study of ionospheric total electron content at crest of equatorial anomaly in China from 1997 to 2007, *Adv. Space Res.*, *50*, 70–76.
- Yamazaki, Y., and M. J. Kosch (2015), The equatorial electrojet during geomagnetic storms and substorms, *J. Geophys. Res. Space Physics*, *120*, 2276–2287, doi:10.1002/2014JA020773.

Unavco Citations

- Bendick, R. (2013a), Ethiopia Tectonics GPS Network: DEBK-Debarek P.S., UNAVCO, GPS Data Set, doi:10.7283/T5Z31WJV accessed 10 May 2016, time-windowed subset 2012-01-01 through 2012-12-31.
- Bendick, R. (2013b), Ethiopia Tectonics GPS Network: SHIS-Shimsheha P.S., UNAVCO, GPS Data Set, doi:10.7283/T5JS9NCX accessed 10 May 2016, time-windowed subset 2012-01-01 through 2012-12-31.
- Bendick, R. (2013c), Ethiopia Tectonics GPS Network: ASOS-Assosa P.S., UNAVCO, GPS Data Set, doi:10.7283/T55H7D6V accessed 10 May 2016, time-windowed subset 2012-01-01 through 2012-12-31.
- Bendick, R. (2013d), Ethiopia Tectonics GPS Network: NEGE-Negele P.S., UNAVCO, GPS Data Set, doi:10.7283/T5B856Z2 accessed 10 May 2016, time-windowed subset 2012-01-01 through 2012-12-31.
- Bendick, R., and R. E. Reilinger (2007a), Ethiopia Tectonics GPS Network: BDAR-Bahir Dar P.S., UNAVCO, GPS Data Set, doi:10.7283/T5TB14TH accessed 10 May 2016, time-windowed subset 2012-01-01 through 2012-12-31.
- Bendick, R., and R. E. Reilinger (2007b), Ethiopia Tectonics GPS Network: NAZR-Nazret P.S., UNAVCO, GPS Data Set, doi:10.7283/T5F18WNH accessed 10 May 2016, time-windowed subset 2012-01-01 through 2012-12-31.
- Bendick, R., and R. E. Reilinger (2007c), Ethiopia Tectonics GPS Network: ARMI-Arba Minch University P.S., UNAVCO, GPS Data Set, doi:10.7283/T59884X5 accessed 10 May 2016, time-windowed subset 2012-01-01 through 2012-12-31.
- Nyblade, A. (2010), Africa Array GPS Network: DODM-Entebbe P.S., UNAVCO, GPS Data Set, doi:10.7283/T5319SZK accessed 10 May 2016, time-windowed subset 2012-01-01 through 2012-12-31.
- Nyblade, A. (2012), Africa Array GPS Network: MTVE-MTWARA P.S., UNAVCO, GPS Data Set, doi:10.7283/T5N014MT accessed 10 May 2016, time-windowed subset 2012-01-01 through 2012-12-31.